The Multibeam Radar Sensor BIRALES: Performance Assessment for Space Surveillance and Tracking

Matteo Losacco, Pierluigi Di Lizia, Mauro Massari
Department of Aerospace Science and Technology
Politecnico di Milano
Via G. La Masa, 34, Milano IT 20089
+39-02-2399-8323
{matteo.losacco, pierluigi.dilizia, mauro.massari}@polimi.it

Germano Bianchi, Giuseppe Pupillo, Andrea Mattana, Giovanni Naldi, Claudio Bortolotti, Mauro Roma
Marco Schiaffino, Federico Perini, Luca Lama
Institute of Radio Astronomy (IRA)
National Institute of Astrophysics (INAF)
Via P. Gobetti, 101, Bologna IT 40129
+39-05-1639-9385
{gbianchi, gpupillo, mattana, gnaldi, c.bortolotti, m.roma, m.schiaffino, f.perini, l.lama}@ira.inaf.it

Alessio Magro, Denis Cutajar, Josef Borg
Institute of Space Sciences and Astronomy
University of Malta
Msida MSD Malta 2080
+356-2340-2340
{alessio.magro, denis.cutajar, josef.borg.11}@um.edu.mt

Ten. Col. G.A.r.n. Walter Villadei and Magg. G.A.r.n. Marco Reali
Force Space Policy Office
Italian Air Force
Viale Dell'Universita, 4, Roma IT 00185`
+39 600-4602/600-5595
{walter.villadei@am, marco.reali@aeronautica}.difesa.it

Abstract— **Near-Earth space has become progressively more crowded in active satellites, inactive spacecraft and debris. Consequently, an international effort is currently being devoted to improving the performance of the network of optical and radar sensors for space objects monitoring. In this regard, the use of the Italian novel BIstatic RAdar for LEo Survey (BIRALES) is investigated in this work. BIRALES sensor exploits a bistatic configuration in which the Radio Frequency Transmitter (RFT) located at Salto di Quirra (Cagliari) plays the role of the transmitter, whereas a portion of the UHF Northern Cross antenna (Bologna) is used as the receiver. The first part of the paper is dedicated to the illustration of the sensor, with a detailed analysis of the multibeam receiver gain pattern. The tailored orbit determination algorithm is described, and a detailed analysis of the algorithm for the reconstruction of the trace of the transiting object within the receiver field of view is offered. The second part of the work illustrates the results achieved with both numerical simulations and observation campaigns. The sensor performance is assessed considering both cases of known and unknown objects, and the results in terms of number of observed objects, as well as accuracy in position and velocity are shown. For all cases, the effect of measurement noise on each single available measurement is investigated. The final part of the paper illustrates the results obtained during the observation campaign of space station Tiangong-1 re-entry. An analysis of the accuracy of the obtained results is carried out, and the potential of BIRALES sensor is highlighted.**

TABLE OF CONTENTS

1. INTRODUCTION

The number of manmade objects orbiting the Earth has dramatically increased during the last decades, posing a serious risk for space-based activities. Most of these objects are classified as space debris and include inactive satellites, discarded launch stages, and fragments originated from satellite breakups and collisions. Several countermeasures have been adopted with the aim of reducing mission related risks and to control the number of objects in orbit. In parallel, specific space programs were started to build the expertise required to manage the challenges posed by the space traffic control problem. Collision risk assessment is performed daily by satellite operators who are provided with conjunction summary messages to support decisions on the execution of collision avoidance manoeuvres [1]. In addition, re-entry predictions of objects are regularly produced to estimate on ground risks [2]. Both collision risk assessment and re-entry predictions rely on the accurate estimation and prediction of the state of the orbiting objects, which are derived from the tracking of the space objects using dedicated optical, radar and laser sensors.

Survey and tracking of objects in Earth orbit is one area where

Figure 1: A view of the Medicina Radio astronomical Station. In the foreground, the Northern Cross.

the European Space Surveillance and Tracking (SST) Support Framework and the European Space Agency (ESA) Space Situational Awareness (SSA) programmes are active, and the implementation of a European network of sensors represents one of the main objectives. In this regard, the Italian Northern Cross radio telescope array has been upgraded to serve the European SST Framework in the frame of the BIstatic RAdar for LEo Survey (BIRALES) sensor [3]. BIRALES uses part of the Northern Cross radio telescope located in Medicina (Bologna, Italy) as the receiver (see Fig. 1). Part of the radio telescope has been refurbished and a digital back end has been implemented to allow beamforming of 32 beams distributed across the receiver field of view (FoV) with an 8-cylinders configuration and 64 beams with a 16-cylinders configuration. When an object transits inside the antenna FoV, the beams are illuminated by the reflected radio wave. Consequently, besides the classical range and Doppler shift measurements, the beam illumination sequence provides an estimate of the transit direction of the object in terms of angular deviation with respect to the nominal receiver pointing direction. The data received from BIRALES are provided as input to a tailored orbit determination (OD) algorithm, which is aimed at computing an estimate of the orbital parameters of the observed object. A numerical simulator of BIRALES has been developed to assess its performance through dedicated simulations. Given a catalogue of space objects, the simulator identifies the passages of all the objects in the sensor FoV during a simulated observation campaign. Then, the simulated measurements are generated for each passage and are provided as input to the OD module, along with the required transmitter and receiver information.

The first part of this paper is dedicated to the description of BIRALES sensor. Then, a detailed illustration of the OD algorithm is offered, with the trace reconstruction algorithm representing the core of the method. Finally, the performance of the sensor is presented as obtained with both numerical simulations and real observation campaigns.

2. BIRALES SENSOR

BIRALES sensor uses a bistatic configuration. The Radio Frequency Transmitter (RFT) located at the Italian Joint Test Range of Salto di Quirra (PISQ) in Sardinia is used as transmitter (Fig. 2), and part of the Northern Cross radio telescope of the radio astronomy station of Medicina as receiver.

The RFT consists of a powerful amplifier able to supply a maximum power of 10 kW in the bandwidth 410-415 MHz.

Figure 2: Radio Frequency Transmitter.

It is a 7 m dish completely steerable at a maximum speed of 3 deg/s and with right-hand circular polarization. Its FoV matches almost perfectly the receiving antenna one, with a beam width of 6 deg. The receiving antenna is a portion of the Northern Cross Radio Telescope (Fig. 3), which is currently one of the largest UHF-capable antennas in the world, being located at the Medicina Radio Astronomical Station, near Bologna, in Northern Italy [4]. It is owned by the University of Bologna but managed and operated by the Institute of Radio Astronomy at the Italian National Institute of Astrophysics (INAF-IRA). It consists of two perpendicular branches: the East-West (E/W) arm is 564 m long and consists of a single cylindrical antenna with a width of 35 m, whereas the North-South (N/S) branch is made of 64 parallel antennas with a length of 23.5 m and width of 7.5 m each.

The portion dedicated to BIRALES receiving antenna is actually composed of 16 parabolic cylindrical antennas of the N/S branch (see Fig. 3). The total collecting area is about 2800 m^2 and it allows the detection of small objects with sub-metric Radar Cross Section (RCS) at 1000 km of altitude. The peculiarity of the receiver is represented by the possibility of detecting meridian passages only, as it can be moved in elevation only. BIRALES works in survey mode and exploits an innovative concept based on a multibeam technique. Due to the large numbers of receivers installed on the Northern Cross (4 receivers in each N/S antenna for a total of 64 receivers), the FoV can be populated with many independent beams. When an object transits inside the antenna FoV,

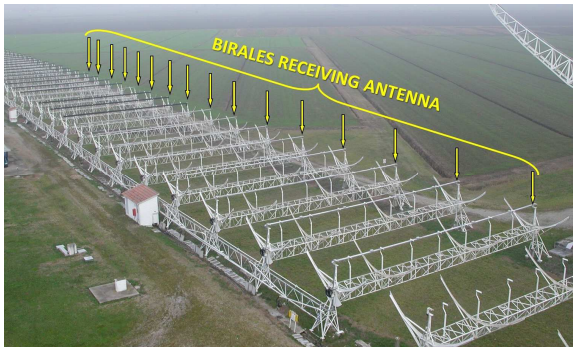

Figure 3: BIRALES receiving antenna.

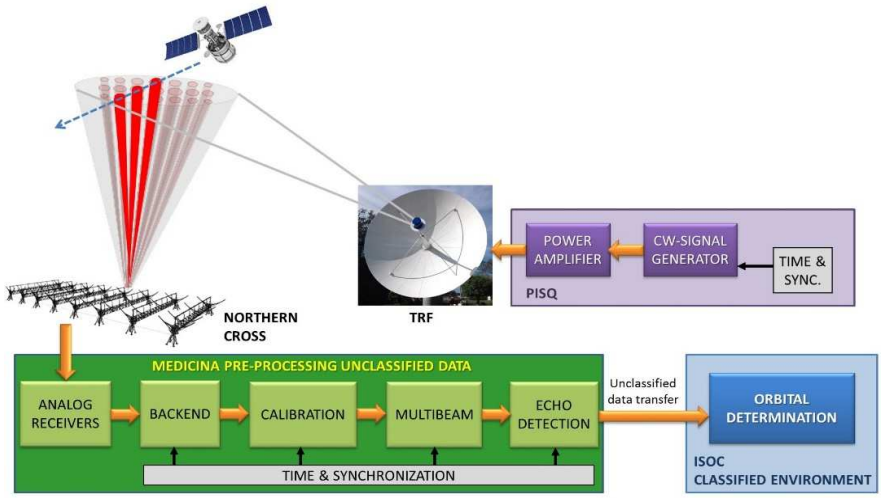

Figure 4: BIRALES system architecture

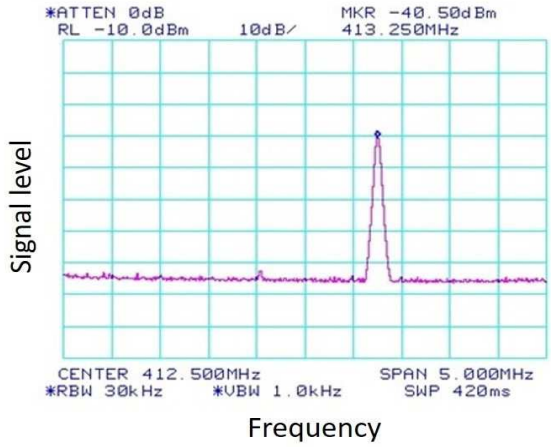

Figure 5: Radio Frequency Interference scenario in the operative bandwidth for BIRALES sensor: signal amplitude vs operative frequency

beams are illuminated by the reflected radio waves. Thus, by looking at the beam illumination sequence, it is possible to estimate the ground track of the transiting objects with a higher level of detail with respect to a single-beam system.

The system architecture is shown in Fig. 4. Using the RFT it is possible to transmit a CW signal able to illuminate the target in LEO. The echo reflected by the orbital object is received through the Northern Cross and the acquired analog signal is sent to the pre-processing room by an optical fiber link. The digitized data are processed by means of a data acquisition system based on FPGA boards and CPUs, which digitally assembles measured radar echoes using an FFT in spatial domain in order to evaluate the signal detected in each beam. Therefore, Doppler shift, illumination time, antenna pointing angles and measured power intensity associated to each beam are available as well and they are sent to the Italian SST Operation Centre (ISOC) to estimate the orbit of the object detected in a classified environment.

Figure 5 shows the Radio Frequency Interference (RFI) scenario in the operative bandwidth for BIRALES sensor.

The plot shows an image of a spectrum analyzer used for interference monitoring in terms of signal amplitude (from -110 dBm to -10 dBm, 10 dBm division) as a function of the operative frequency (410-415 MHz, 0.5MHz division). The sweep time (SWP) of every spectrum shown in the spectrum analyzer is 420 ms, with 30 kHz of resolution bandwidth (RBW) and 1 kHz of video bandwidth (VBW). The Italian bandwidth 410-430 MHz is assigned to the Ministry of Defence for fixed and land mobile service. Some interference occasionally appears, as the one reported in the plot at 413.25 MHz. Its power peak is -40 dBm, but, since the gain of the receiver chain (from the RFI monitoring antenna to the spectrum analyzer) is 55 dB, the real power of the received signal is 95.5 dBm. Moreover, the echo signals of orbiting objects are characterized by Doppler shifts, and this allows one to easily distinguish these signals from the ones emitted by terrestrial transmitters.

The sensor has been recently upgraded in order to provide also range measurements. Radar ranging works by transmitting, along with the carrier wave, a chirp of known period and span. The Doppler shift can be estimated by the carrier reflection, and the knowledge of this correction for the underlying chirp and of the transmission epoch provides a time of flight. The estimated time of flight is however affected by an ambiguity of N chirp periods. A detailed description of the whole receiver architecture is offered below.

Analog Receiver

The radio echo received by the Northern Cross is amplified by a front-end board installed on the antenna focal line. The box contains also one electro-optical converter which transmits the analog signal to the pre-processing room by means of the optical fiber link. The front-end performances are:

- NF = 0.45 dB, Tn = 32 K
- Gain = 60 dB
- BW = 16 MHz @408 MHz
- OIP3 > +33 dBm
- InputRL > 15 dB
- OutputRL > 15 dB
- PowerSupply = (10-15) Volt @245 mA

The measured parameters for 64 optical links (@400 MHz) are:

- |S11| < -16 dB
- |S22| < -17 dB
- Gain = 2 dB ±1
- Noise figure < 35 dB
- OIP3 > 35 dBm
- OIP2 > 47 dBm

Back end

The back end system acquires 64 analog signals coming from 64 antenna receivers that need to be digitized by 64 Analog to Digital converters (ADCs). The analog band at the ADCs inputs is 16 MHz centred at 30 MHz (down converted frequency). The data sampled are sent to a first FFT block in order to generate channels with a sample resolution of 78 KHz, that is the maximum space debris Doppler shift. The BIRALES system requires a real-time processing back end that can perform fine channelization of the incoming antenna voltages, pixelate the FoV with multiple coherent beams and process each of these beams for detection of debris echoes. Accurate beam pointing requires the calibration of the array of antennas. Additionally, the system shall be capable of storing and visualizing the results, as well as transmitting them to the orbit determination system. In order to accommodate all these processing stages whilst enabling the addition of new stages with ease, a framework for generating processing pipelines was developed for BIRALES. The pipelining framework makes up the real-time software back end. This framework allows for the chaining of different software modules into pipelines, the main ones being:

- The calibration pipeline, which receives data from the digital back end and correlates the antenna signals together to generate correlation matrices. These are then used by the calibration routine to generate calibration coefficients to compensate for instrumental phase and gain errors.

- The real-time processing pipeline, which receives data from the digital back end, performs beamforming and channelization and either writes the resulting data to file or forwards it to the online detection modules for debris detection.

Calibration

Both geometric and inherent instrumental delays will interfere with the true sky visibilities, rendering the visibilities measured by the respective antennas out of phase. This directly results in a reduced signal-to-noise ratio (SNR) as a result of destructive interference occurring in the out of phase fringe patterns obtained from correlating the respective antenna visibilities.

While the geometric delays as a result of the position of the antennas in the field in relation to the position of the measured radio source can be easily derived, the same cannot be said for the inherent instrumental delays which might change as a result of a number of factors. Because of the unpredictability and changing nature of such instrumental delays, a simple but robust instrumental calibration is essential for reducing the resulting lowered sensitivity of an otherwise uncalibrated array. The solution proposed here for the BIRALES receiving array aims to allow calibration to be carried out on a strong point source of relatively stable flux emission in order to characterize instrumental delays. The BIRALES array antennas can only be slewed in altitude, meaning that observation of potential calibration sources can be achieved by slewing to the sources declination and waiting for the target to transit.

The observation would thus be carried out at the time where the source Right Ascension (RA) is equivalent to the local sidereal time. For this reason, the observed incoming visibilities as a source begins transiting the primary beam are expected to change according to the position of the source in the beam itself, as there is no sidereal tracking undergone. Due to both geometric and instrumental effects, the expected clean bell-shaped peak of the transit visibilities of a strong point source are not however achieved, as the incoming visibilities are out of phase as aforementioned. However, it is known that for a given transit of such a source across the field of view, phase differences between the visibilities of the antennas should be zero when the source is exactly in the beam zenith, that is, exactly when the source is halfway through the transit.

Stage 1: Peak Source Transit Time Determination—After an observation of a strong source transit, a peak power search is carried out in the correlated visibilities to identify the peak transit of the source through the instruments beam zenith. The recorded visibilities from all the antennas at each time interval are investigated, in order to determine the time interval at which peak power for the entire transit was measured.

Stage 2: Peak Visibilities Calibration—The array visibilities measured at the peak transit time can thus be identified. Subsequently, per-baseline coefficients are obtained for peak visibilities, which give the expected equal gain and phase values for all visibilities at peak transit. The per-antenna coefficients are then obtained by assuming a reference antenna with zero calibration requirements, and obtaining calibration coefficients for all other antennas with respect to it. In order to eliminate possible anomalous antennas interfering with the calibration procedure, all antennas for which coefficients vary beyond a threshold from the rest of the coefficients are left uncalibrated. The calibration coefficients obtained at this stage, however, still incorporate corrections for both instrumental and geometric effects, the latter making them valid only for the declination pointing of the calibrator source in question.

Stage 3: Geometric Effects Subtraction and Subsequent Addition—The final stage in obtaining the instrumental calibration coefficients involves the separation of geometric effects, which is obtained by subtracting geometric corrections from the calibration coefficients obtained. After their removal, the resulting coefficients represent the true corrections required to counter inherent instrumental effects only. These coefficients are then fed back to the real-time processing pipeline.

Multibeam

The multibeam pipeline performs fine channelization and multibeaming, generating multiple beams within the primary field of view of the array. The resulting beams are then processed by the detection module, which searches for space debris echoes. This pipeline is composed of three software modules: receiver, channelizer, beamformer.

Receiver—The digital back end transmits data to the software back end over a 10 Gb link, containing a single ~78k Hz coarse channel from the 64 antennas. They are transmitted in 32+32 complex fixed point format, which needs to be translated to floating point format. The AAVS DAQ library was extended to accept the BIRALES data format and encapsulated as a module. This will read incoming data in chunks and forward the data to the subsequent processing module.

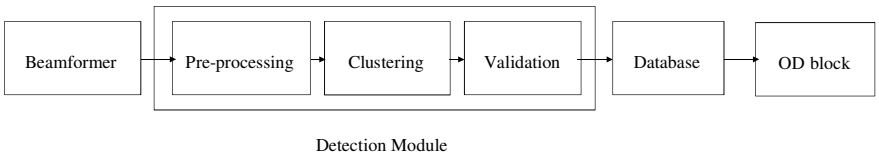

Figure 6: The main stages of the BIRALES Data Detection Module.

Channelizer—The channel bandwidth is too wide for debris detection, so finer channelization is required. This module implements a polyphase filter bank channelizer, splitting the channel into 8192 ~9.5 Hz separate channels, allowing for a temporal resolution of ~10 samples/s. The number of taps is configurable (more taps require more processing), and each antenna is processed by several threads in a thread pool.

Beamformer— The beamformer generates the multi-pixel, which fills the primary field of view with coherent beams, allowing the tracing of debris through the beam. The beam pointing coefficients are static since no tracking is required and the beam configuration does not change during an observation. The number of beams to generate and their pointing within the primary beam are configurable.

Echo Detection

The final stage of BIRALES space debris pipeline is the data detection module. The aim of this module is to analyse the beamformed data provided by the beamformer module and identify and extract potential space debris candidates. These candidates are put into a database to be later retrieved by the orbit determination block. The main stages of the detection module are illustrated in Fig. 6 and described in the following sections. A more detailed description can be found in [5].

Pre-processing—The beamformed data, which is encoded as complex voltages, is converted into SNR values. An estimate for the background noise value of the system is calculated by taking the average power value of half of the frequency band for a number of samples before the transmitter is initialized. This is then used as the new estimate for the noise. This input is subsequently passed through a number of filters. The aim of the filters is to reduce the number of data points that the detection algorithm has to process. In the first filter, the background noise is filtered out by considering data points that are two standard deviations away from the mean as being noise. This procedure effectively removes the bulk of the data given that most of the data being processed is noise. Secondly, the artefacts introduced by the transmitter are removed by applying a transmission line filter, which applies a threshold on those channels in which a time-independent high SNR is recorded. This ensures that the transmission frequency is not considered by the detection algorithm. The resulting data could still be noisy. These data are usually characterized by random isolated clusters of data points with a low SNR. These data points, or pixels, can be removed through binary hit-ormiss transform. This transform finds the pixels which match a specified pattern or mask. The mask is a representation of a single pixel with no immediate neighbouring pixels.

The application of the aforementioned three filters proved to be very effective in clipping most of the noise thereby reducing the complexity of the detection algorithm. However, some noise can still be present after this filtering process. Thus, the detection algorithm needs to be robust enough to cater for any noise artefact after the filtering stage.

Clustering Algorithm—The DBSCAN clustering algorithm is used to cluster data points. It is an unsupervised algorithm that works by grouping points that are closely packed together, expanding clusters in any direction where there are nearby points. This way, it is able to deal with different shapes of clusters. Furthermore, it is robust to noisy data, making it an ideal clustering algorithm to be used for this application [6]. The algorithm is applied to each beam data separately in parallel. The clusters identified by this algorithm are then determined to be potential beam candidates.

Validation of the Beam Candidates—The beam candidates are then validated by a number of criteria. The shape of the space debris detection cluster is expected to be linear. Thus, the next stage of the detection module is to identify "linear clusters". The algorithm looks for clusters with a high degree of correlation between frequency and time. In order to do so, the RANdom SAmple Consensus (RANSAC) regression algorithm is used [7]. RANSAC gives a smaller weight to outlier data points, meaning that these data points are ignored. Furthermore, data points that are highlighted as being outliers are removed by the detection algorithm. This means that we not only end up with higher quality clusters (linear clusters with no noise) but it also means that clusters that were eliminated previously because of that data point are no longer deleted. Another optimization that was introduced was to ignore clusters with an unrealistic Doppler shift value. Analysis of the catalogued objects in orbit put the expected Doppler shift Δf to lie between -19688 and +19507 Hz. The values were obtained by performing numerical simulations covering one week of observations for the whole NORAD catalog and estimating the measured Doppler shift value at the meridian passage. Clusters with a Doppler shift value outside this range are dropped. Similarly, a range for the rate of change in the Doppler shift of the detection was obtained. The rate of change in the measured Doppler is expected to lie between -851 and -1 Hz/s according to numerical simulations. This process ensures that only valid object tracklets are considered. The remaining validated clusters are then pushed to the space debris queue. The space debris queue is a data structure which was built to hold the validated space debris clusters being identified by the detection algorithm. This data structure ensures that data from the same space debris target are merged into a single space debris object. When the state of the queue changes (by addition or deletion), the space debris candidates are put into the database. Candidates that were not modified are not saved again. Once the candidates are put into the database, the user is able to visualize the detections through the monitoring application in real-time. At the end of an observation, the detections made are saved in a Tracking Data Message (TDM) format that can be used by orbit determination routines.

3. ORBIT DETERMINATION

The starting point for the OD algorithm implemented for BIRALES sensor is represented by a TDM measurement file including, for all the beams illuminated during the object passage, the epoch and the recorded slant range, Doppler shift and SNR measurements. Then, the algorithm is divided in two parts. The first part is dedicated to the estimation of the trace of the object inside the receiver FoV starting from the available SNR and slant range measurements. Then, the state of the object is estimated on the basis of the available slant range and Doppler shift measurements and the estimated trace. In the following paragraphs, both phases are described in detail. The analyses are performed considering the current 8-cylinders configuration (32 beams) and slant range measurements available.

Trace definition

The peculiarity of BIRALES sensor is the possibility of populating its receiver field of view with 32 beams in the 8-cylinders configuration. Figure 7 shows the distribution of the 32 beams within the receiver FoV. The angles $\Delta\gamma_1$ and $\Delta\gamma_2$ represent the angular deviations with respect to

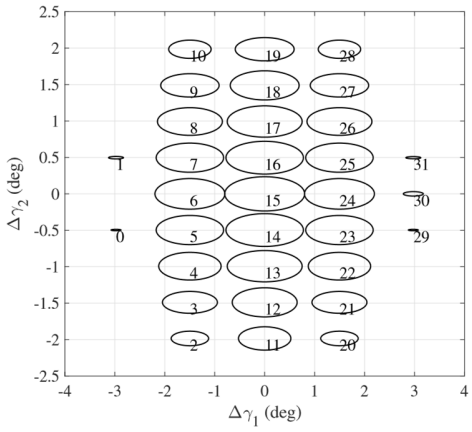

Figure 7: Medicina 8-cylinders receiver beam pattern in terms of angular deviations $\Delta\gamma_1$ and $\Delta\gamma_2$.

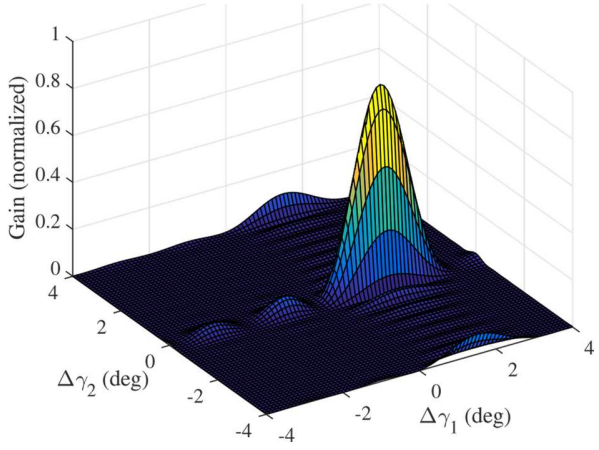

Figure 8: Gain pattern for beam 24: one main lobe, and other minor side lobes.

the receiver nominal pointing. Each single beam typically presents a main lobe, some side lobes and may present the so called "grating lobes", which are generated by the geometry of the array itself. The entity of these grating lobes may be more or less significant according to the investigated beam. The gain pattern of each single beam mainly depends on its position inside the receiver FoV. Beams located close to the line of sight of the sensor typically show only a main lobe and side lobes, whose size is much lower than the size of the main lobe. An example is given in Fig. 8 for beam 24, with one main gain peak and other secondary, much weaker, side lobes. These beams will be defined throughout the paper as "dominant beams". On the contrary, beams located at the boundaries of the FoV typically have one lobe, a grating lobe, whose gain is comparable with the one of the main lobe. Figure 9 shows the gain pattern for beam 30: as can be seen, given the main lobe, there is another gain peak whose size can be compared with the main lobe, and there are other not negligible secondary peaks.

The peculiarity of the receiver gain pattern has obviously a strong impact on the approach followed in the definition of the object trace inside the receiver FoV. The idea at the basis of the approach is to reconstruct the trace of the object by looking at the sequence of illumination of the beams. This, in turn, essentially consists in matching the measured SNR profile with the one obtained by estimating the trace inside the field of view. The algorithm can be divided in two phases: a first phase S1, in which a first estimate for the object trace is obtained by looking at the recorded SNR peaks, and a second phase S2, in which the obtained trace is used as a first guess for a least-squares fit aimed at minimizing the residuals with respect to the whole SNR profile of all the illuminated beams.

The definition of the first guess S1 is done by looking at all the SNR peaks recorded during the passage of the object and associating each signal peak to a given gain peak of a specific beam. This probably represents the most challenging aspect of the trace definition algorithm, given the presence of multiple gain peaks per beam. When one beam is illuminated, indeed, it is not straightforward to understand which gain peak is responsible for the beam illumination. It is therefore necessary to identify some SNR peaks that are likely to be associated to specific gain peaks. The idea behind the implemented approach consists in starting the process by

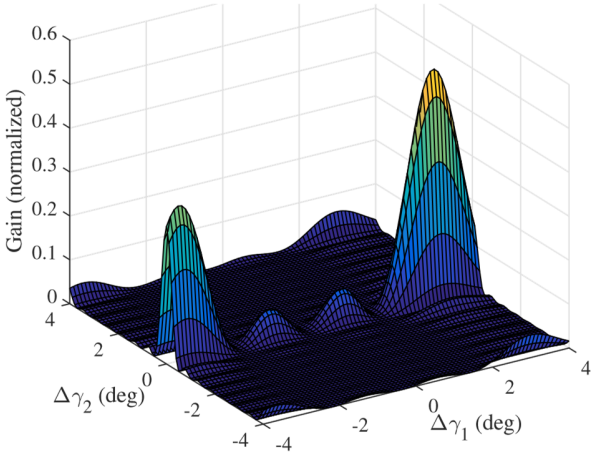

Figure 9: Gain pattern for beam 30: one main lobe, a grating lobe and other not negligible side lobes.

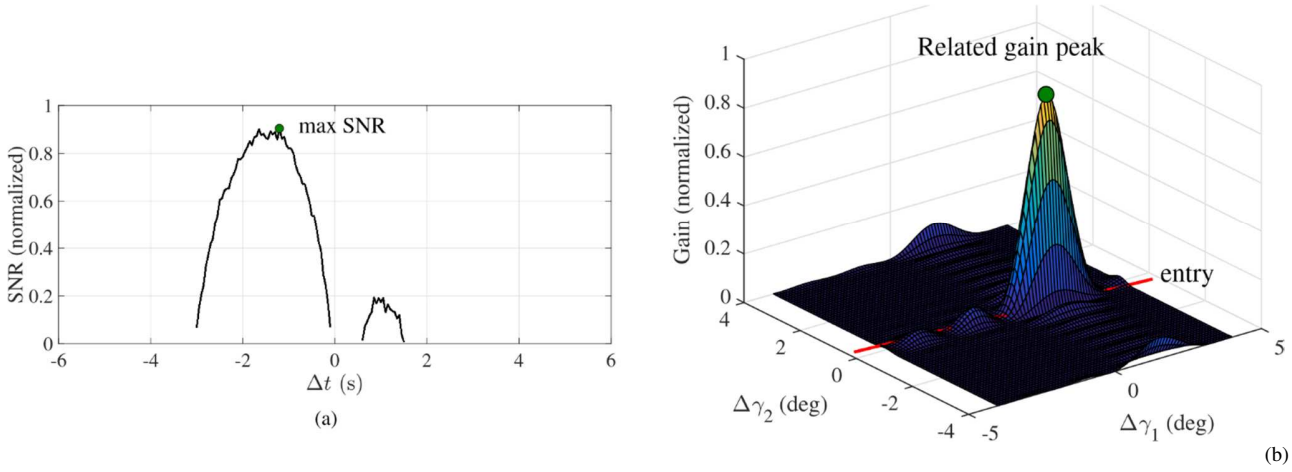

Figure 10: Dominant beams signal peaks association phase for beam 24: (a) SNR profile and signal peak as a function of the time delay with respect to the expected meridian passage Δt, (b) gain pattern profile and associated gain lobe.

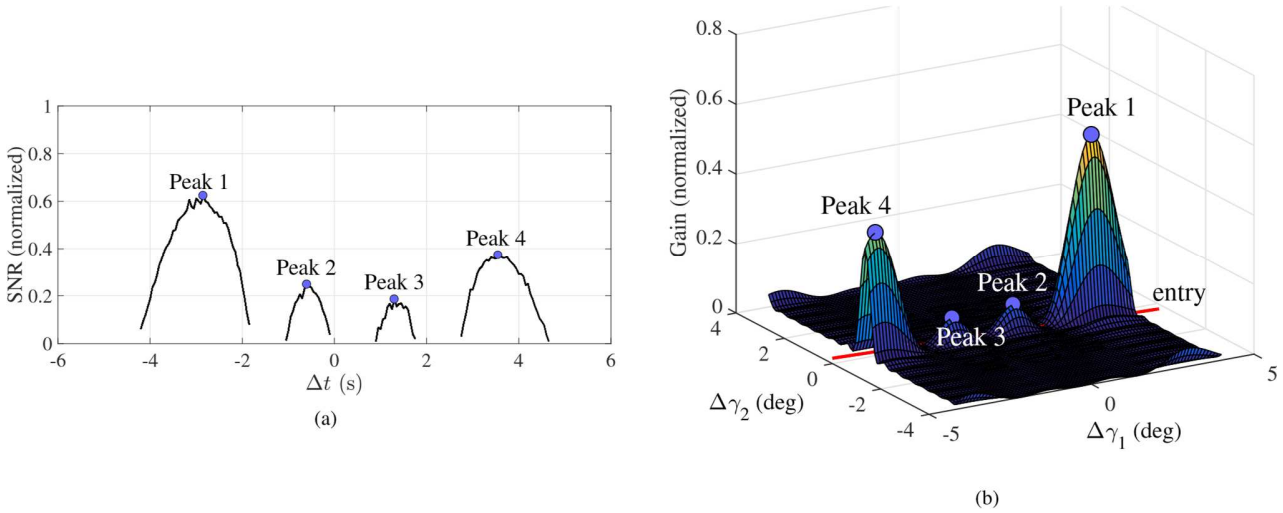

Figure 11: All beams signal peaks association phase for beam 30: (a) SNR profile and signal peaks as a function of the time delay with respect to the expected meridian passage Δt, (b) gain pattern profile and associated gain lobes.

considering the largest SNR peak recorded by each dominant beam. When one of these beams is illuminated, its maximum signal peak is automatically associated to the main lobe of the beam in terms of angular deviation. Figure 10 shows the signal association process for beam 24, obtained performing a numerical simulation of the passage of object NORAD ID 41765 on April 20, 2018, at 12:41:38.34 UTC: once the whole SNR profile has been recorded, the maximum SNR peak is isolated, and it is associated with the main gain lobe of that beam. By assuming a linear trend in time of the angular deviation profiles $\Delta\gamma_1(t)$ and $\Delta\gamma_2(t)$ and performing a first polynomial fit, this allows us to obtain a first estimate of the trace of the object inside the receiver FoV. Once this trace is defined, we can start considering all SNR peaks, including the ones of beams with multiple comparable gain peaks, and we can associate each signal peak to a specific gain peak by identifying the lobe with minimum deviation with respect to the previously estimated trace at the epoch the SNR peak was detected. Figure 11 shows the result of the signal association process for beam 30: four signal peaks are detected, and the corresponding gain lobes are retrieved. This procedure provides us with a full list including, for each recorded signal peak, the corresponding time epoch and angular deviations of the associated gain peaks. These data are processed with a new linear fit, and a refined first guess for the object trace is obtained.

The described approach allows us to maximize the information extracted from the beam illumination sequence by simply looking at the recorded SNR peaks and exploiting the gain pattern. This procedure does not require any other measurement apart from the SNR. If slant range measurements are also available, then a further step can be performed. Starting from the estimated object trace, and assuming a polynomial trend of the angular deviations with time, by knowing the slant range measurements at each observation instant it is possible to perform a least-squares fit aimed at minimizing the residuals with respect to the whole SNR profile of all beams.

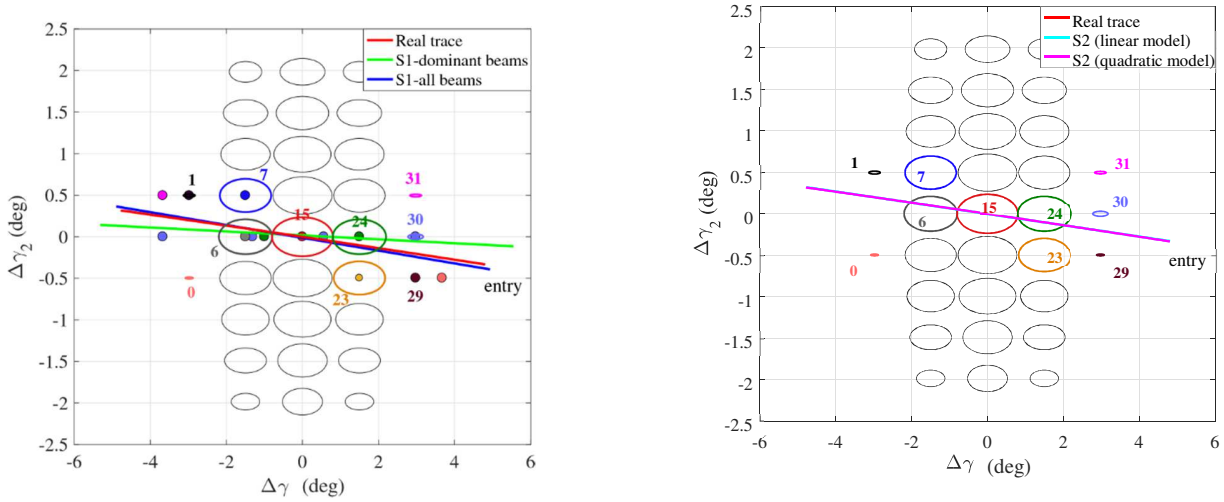

Figure 12: Trace definition for object NORAD ID 417654, passage on April 20, 2018: (a) step S1, trace definition based on SNR peaks, (b) step S2, nonlinear least-squares on the whole SNR profiles.

This second step, referred to as S2, allows us to increase the accuracy of the estimate and concludes the trace definition phase. Figure 12 shows the results of the trace definition phase for object NORAD ID 41765, April 20, 2018. The real trace of the object is shown in red. Figure 12a shows the results of step S1. The estimated trace obtained considering the largest SNR peaks of the dominant beams only (beams 6, 7, 15 and 24) is shown in green. The final result of step S1 is shown in blue: as can be seen, by considering all the SNR peaks, the accuracy of the estimate significantly increases. Figure 12b shows the estimated trace obtained with step S2, considering a linear (cyan) and quadratic (magenta) trend in time of the angular deviations: the availability of the slant range allows us to obtain a further improvement in the definition of the trace, getting to an estimate almost overlapping the real trace.

The described algorithm is valid in both cases of known object (i.e. object whose Two-Line Elements (TLE) is available) and unknown object. In the case of known object, the availability of the TLE gives us an a priori estimate of the possible path in the receiver FoV. This estimate can be exploited to ensure convergence of step S2 in all those situations in which the passage of the object is critical. These situations occur every time symmetry conditions occur. Symmetry conditions appear when a single column of gain peaks is illuminated. In such cases, the output of step S1 is a straight line connecting these lobes. If this is the case, the initial guess is exactly halfway between the real solution and a symmetric one which gives the same SNR profile, but a wrong trace in the FoV. If the object is known, convergence can be granted by deviating the initial guess of step S1 in the direction of the trace predicted by the TLE. The situation becomes more critical if the object is unknown. In this case, two possible solutions exist. The algorithm, therefore, cannot distinguish the right one, and needs to store both.

Object state estimation

The output of the trace definition phase is a value of $\Delta\gamma_1$ and $\Delta\gamma_2$ for each observation instant. These two estimates, along with the Doppler shift and slant range measurements, are used to estimate the state and covariance of the object at the epoch of the first observation. The estimation is done with a Levenberg-Marquardt least-squares batch algorithm and requires an accurate model for the object dynamics. The considered high-fidelity propagator, called AIDA (Accurate Integrator for Debris Analysis), includes the gravitational model EGM2008 up to order 10, the atmospheric drag with the atmosphere model NRLMSISE-00, third body perturbations, and solar radiation pressure with a dual-cone model for Earth shadow for objects whose geometrical parameters are known. For unknown objects, only gravitational and thirdbody effects are considered.

4. RESULTS

The analysis of the performance of BIRALES sensor is presented in this section. The first part is dedicated to the results of numerical simulation, whereas the second part shows the results obtained during the observation campaign performed for the re-entry of the space station Tiangong-1.

Numerical simulations

In order to assess the performance of the BIRALES sensor we carried out a numerical simulation using a dedicated sensor simulator. Starting from a catalogue of available objects, the simulator computes, for each object, the predicted passage epoch and simulates the behaviour of BIRALES sensor generating the measurements in terms of slant range, Doppler shift and SNR. Further details about the behaviour of the simulator are given in [8]. We considered an observation window of two days, covering the range 5-6 September 2018, with 2490 objects with at least one passage, and for all these objects we analysed the first passage only. The characteristics of the sensor in terms location (latitude, longitude and altitude) and power are shown in Table 2.

Table 1: BIRALES OD performance for both cases of known and unknown objects.

Object	Noise	#objects	$\bar{\varepsilon}_p$(km)	$\bar{\varepsilon}_v$(km/s)	$\bar{\sigma}_p$(km)	$\bar{\sigma}_v$(km/s)
Known	-	44	5.34e-4	1.30e-4	7.80e-5	7.00e-6
Known	DS and SR	44	7.37e-3	2.45e-3	6.24e-2	7.45e-3
Known	DS, SR and SNR	43	6.52e-2	1.24e-2	7.14e-2	8.68e-3
Unknown	-	29	1.29e-3	2.07e-4	4.84e-4	3.50e-5
Unknown	DS and SR	30	7.87e-3	2.91e-3	6.78e-2	5.38e-3
Unknown	DS, SR and SNR	27	5.39e-2	1.32e-2	7.47e-2	4.38e-3

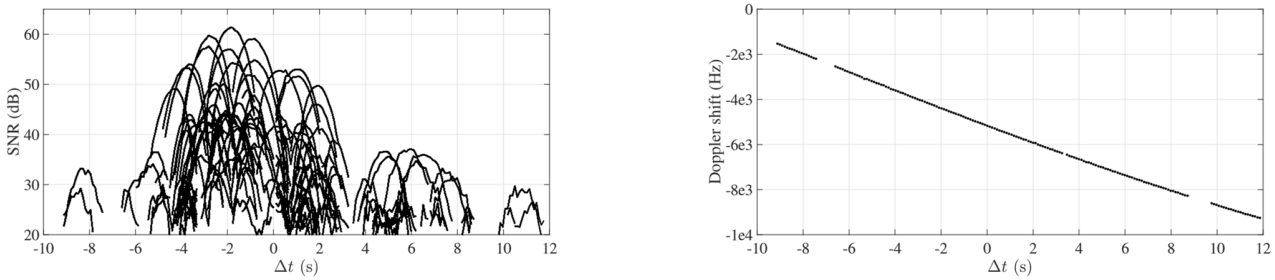

(a) (b)

Figure 13: SNR (a) and Doppler shift (b) measurement profiles obtained during Tiangong-1 passage on March 29, 2018 as a function of time delay Δt (s) with respect to the TLE-predicted passage epoch.

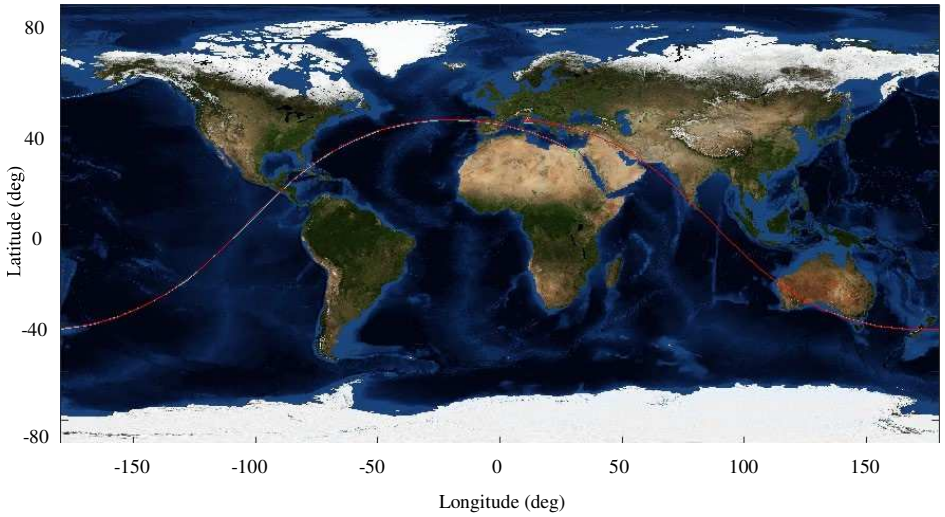

Figure 14: Tiangong-1 trace comparison between OD (cyan) and TLE (red) estimates for March 29.

Table 2: RFT and Medicina receiver locations.

	Lat	Lon	Alt	P
TX	39°36'18"N	9°26'23"E	550 m	10 kW
RX	44°31'14"N	11°38'59"E	28 m	-

We performed the analysis considering both cases of known and unknown objects, assuming the following levels of measurement noise: 3 m of standard deviation for the slant range (SR), 9 Hz of discretization for the Doppler shift (DS), and a white Gaussian noise for the SNR, assuming a ratio of 30 dB between the nominal signal and the added white noise. The results are shown in Table 1. The performance is expressed in terms of mean position and velocity errors $\bar{\varepsilon}_p$ and $\bar{\varepsilon}_v$ and mean standard deviations $\bar{\sigma}_p$ and $\bar{\sigma}_v$.

By analysing the number of observable objects, it is quite evident that this value is quite low. This is partly due to our decision of selecting the first passage only, and partly to the peculiarity of the sensor of detecting meridian passages only with a narrow field of view. Let us now analyse the performance and consider the results for the case of known objects: as can be seen, if we do not add any kind of additional measurement noise, the accuracy granted is very

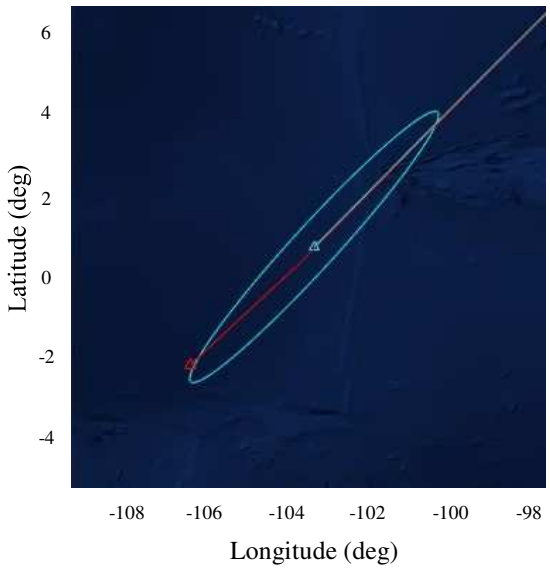

Figure 15: Estimated uncertainty region (cyan) vs TLEpredicted position (red) on March 29, 2018 at 09:00:36.79 UTC

Table 3:BIRALES pointing directions for March 29, 2018.

Epoch (UTC)	Az_{RX} (°)	El_{RX} (°)	Az_{TX} (°)	El_{TX} (°)
07:56:03.27	180.00	40.83	28.80	25.61

Table 4: Keplerian parameters comparison (March 29, 2018 07:55:54.35 UTC).

	a(km)	*e*	*i*(°)	**Ω**(°)
TLE	6567.96	0.0012	42.66	218.04
OD	6558.75	0.0028	42.65	217.96

high, leading to a mean position error that is less than 1 m. If measurement noise is considered, the performance decreases, with an average decrease in accuracy of around two orders of magnitude in both position and velocity. Still, the average position error is lower than 100 m, whereas the average velocity error is slightly larger than 10 m/s.

On the other hand, for unknown objects, the number of objects for which we could univocally provide an OD estimate decreases with respect to the case of known object, whereas the average accuracy in both position and velocity is more or less the same. This result is expected, as when the object is unknown, the trace definition algorithm is prone to symmetry problems. In this case, the only way consists in considering both possible solutions.

Tiangong-1 re-entry observation campaign

In this second part of the section, we show the results obtained during the observation campaign of Tiangong-1 re-entry. The Chinese space station completed its re-entry on April 2, 2018 at 00:16 UTC. During the final week, BIRALES sensor was able to observe the space station several times. In the following paragraphs, we show the results obtained with the observations performed on March 29 and 31.

In both Table 5: BIRALES pointing directions for March 31, 2018.

Epoch (UTC)	Az_{RX} (°)	El_{RX} (°)	Az_{TX} (°)	El_{TX} (°)
06:54:11.61	180.00	38.78	28.54	23.40

Table 6: Keplerian parameters comparison (March 31, 2018 06:53:59.29 UTC).

	a(km)	*e*	*i*(°)	**Ω**(°)
TLE	6551.48	0.0009	42.67	205.05
OD	6538.00	0.0023	42.67	205.27

In both observations the sensor provided only Doppler shift and SNR measurements.

Table 3 shows the sensor pointing directions for the first considered passage in terms of azimuth (Az) and elevation (El) and the meridian passage epoch predicted on the basis of the latest TLE available, whereas Fig. 13 shows the SNR and Doppler shift profiles as a function of the time delay with respect to the predicted meridian passage epoch. As can be seen from the SNR maximum peak, the meridian passage occurred around 2 s in advance with respect to what was expected. Given the unavailability of the slant range, the trace of the object was estimated just relying on step S1, only considering the SNR peaks. The obtained angular deviation estimates were coupled with the measured Doppler shift, and a least-squares fit was used to obtain an estimate of the state of the object at the epoch of the first observation. Figure 14 shows the comparison between the estimated trace (cyan) and the one provided by the latest TLE for one satellite orbit. A comparison between the estimated orbital parameters (semi-major axis *a*, eccentricity *e*, orbital plane inclination *i* and right ascension of the ascending node **Ω**) is shown in Table 4. As can be seen, the most significant differences can be detected in the orbital eccentricity and the semimajor axis, whereas both inclination and right ascension of the ascending node are very similar. Figure 15 shows the comparison between the object trace estimates provided by the propagation of the OD estimate and related covariance (cyan) and the subsequent TLE (red) at the epoch at which the new TLE was released (09:00:36.79 UTC): as can be seen, the TLE prediction lies at the boundaries of the estimated uncertainty regions. That is, the OD estimate is capable of including the new TLE estimate.

A second passage was detected on March 31, 2018. Table 5 shows the TLE-predicted pointing directions and the expected meridian passage epoch. In this case, the difference between the TLE prediction and the real passage was more significant (around 7 s), as can be seen by looking at the recorded SNR and Doppler shift profiles (Fig. 16). This yielded a more evident difference between the orbital parameters provided by the TLE and the estimated ones, as shown in Table 6.

Starting from the available state estimates, an estimate for the re-entry epoch was obtained by propagating them forward in time. Figure 17 shows the evolution in time of the predicted re-entry window, provided by the European Space Agency. On the same plot, the re-entry estimates obtained with the observations of March 29 and 31 are shown. As can be seen, while the first estimate is out of the predicted window, the estimate obtained with the observation of March 31 is well included in the predicted re-entry window.

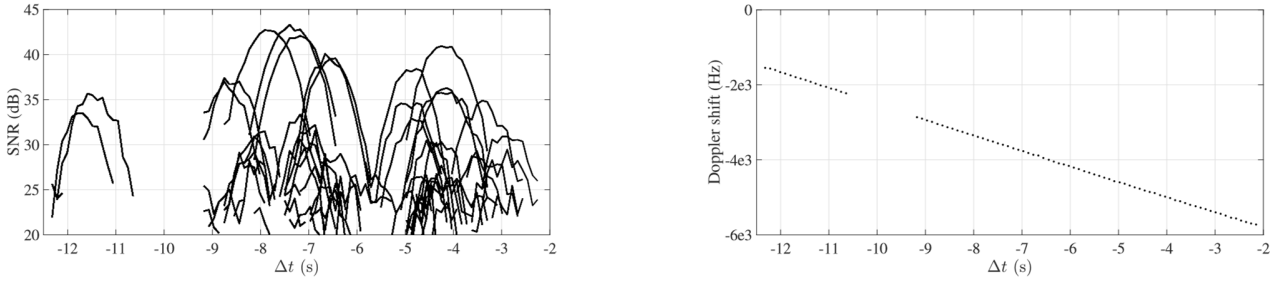

(a) (b)

Figure 16: SNR (a) and Doppler shift (b) measurement profiles obtained during Tiangong-1 passage on March 31, 2018 as a function of time delay Δt (s) with respect to the TLE-predicted passage epoch.

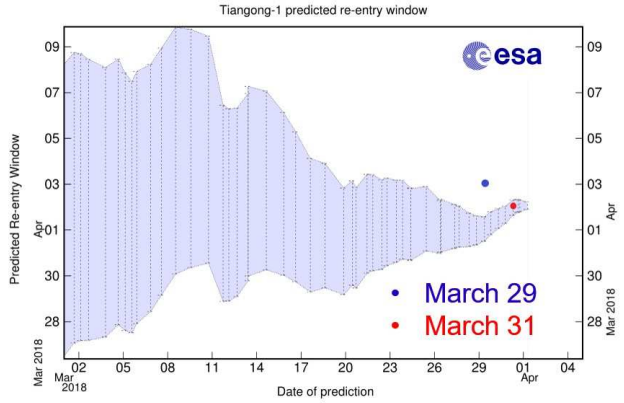

Figure 17: Estimated re-entry window for space station Tiangong-1.

While the orbit determination accuracy for both cases was the same, the required propagation window was different, and this is the main reason for the results shown in Fig. 17. This result is however important, since it shows that BIRALES sensor can provide sufficiently accurate results even with only Doppler shift and SNR measurements starting from the estimates of a single object passage. Considering the current availability of additional slant range measurement, we are confident that the good performance shown by the sensor will be further improved in future observation campaigns. In any case, the obtained results show that BIRALES sensor could play an important role in the framework of a national and European sensor network.

5. CONCLUSIONS

BIRALES sensor represents an innovative radar sensor within the European SST framework. This paper illustrated in detail the system architecture, as well as the innovative orbit determination algorithm developed for BIRALES. The performance of the sensor in terms of achievable accuracy of the orbital estimation process on a catalogue of resident space objects has been assessed through numerical simulations. The sensor can estimate the orbital states with reasonable accuracy with just a single pass for both cases of known and unknown objects. The latter represents the most critical one, as sometimes symmetry problems lead to two possible solutions. The results obtained during space station Tiangong1 re-entry observation campaign were shown, and the good agreement between predicted and estimated object state was highlighted. Future developments include the testing of the sensor including slant range measurements, and the possible coupling with other Italian and European sensors.

ACKNOWLEDGMENTS

The authors acknowledge the support of the Italian Space Agency and the Italian National Institute of Astrophysics through the grant agreement n. 2015-028-R.O. (Space Debris IADC activities support and SST pre-operative validation). The research activities and operations described in this paper were performed within the European Commission Framework Programme H2020 and Copernicus "SST Space Surveillance and Tracking" contracts No. 785257-23SST2016 and No. 237/G/GRO/COPE/16/8935-1SST2016.

The Radio Frequency Transmitter is a facility of the Italian Air Force, located at Italian Joint Test Range of Salto di Quirra in Sardegna. The Northern Cross Radio Telescope is a facility of the University of Bologna operated under agreement by the IRA-INAF (Radio Astronomy Institute National Institute of Astrophysics). The authors acknowledge Daniele Antonio Santeramo from Politecnico di Milano for his contribution to the graphical elaboration of Tiangong-1 re-entry OD results.

REFERENCES

[1] T. Flohrer, H. Krag, S. Lemmens, B. Bastida Virgili, K. Merz, and H. Klinkrad, "Statistical look on ESA's conjunction event predictions," in *Proc. of the 6th Europ. Conf. on Space Debris*, 2013.

[2] C. Pardini and L. Anselmo, "Re-entry predictions of three massive uncontrolled spacecraft," in *23rd International Symposium on Space Flight Dynamics*, Pasadena, 2012.

[3] A. Morselli, P. Di Lizia, G. Bianchi, C. Bortolotti, S. Montebugnoli, G. Naldi, F. Perini, G. Pupillo, M. Roma, M. Schiaffino, A. Mattana, E. Salerno, A. Magro, K. Z. Adami, R. Armellin, A. L. Sergiusti, W. Villadei, F. Dolce, M. Reali, and J. Paoli, "A new high sensitivity radar sensor for space debris detection and accurate orbit determination," in *Metrology for Aerospace (MetroAeroSpace)*, 2015.

[4] S. Montebugnoli, G. Bianchi, J. Monari, G. Naldi,

F. Perini, and M. Schiaffino, “BEST: Basic Element forSKA Training. Wide Field Science and Technology for the Square Kilometre Array,” in *Proc. Of the SKADS Conference*, 2009, pp. 331–336.

[5] D. Cutajar, A. Magro, J. Borg, K. Z. Adami, G. Bianchi, C. Bortolotti, L. Lama, A. Mattana, G. Naldi, F. Perini, G. Pupillo, M. Schiaffino, P. Di Lizia, M. Losacco, M. Massari, M. Reali, and W. Villadei, “A real-time space debris detection system for BIRALES,” in *Proc. of the 69th International Astronautical Congress*, 2018.

[6] M. Ester, H.-P. Kriegel, J. Sander, and X. Xu, “A densitybased algorithm for discovering clusters in large spatial databases with noise,” in *KDD-96 Proceedings*, vol. 96, no. 34, 1996.

[7] M. A. Fischler and R. C. Bolles, “Random sample consesus: a paradigm for model fitting with applications to image analysis and automated cartography,” *Communications of the ACM*, vol. 24, no. 6, pp. 381–395, 1981.

[8] M. Losacco, P. Di Lizia, M. Massari, A. Mattana, F. Perini, M. Schiaffino, C. Bortolotti, M. Roma, G. Naldi, G. Pupillo, G. Bianchi, D. Cutajar, A. Magro, C. Portelli, M. Reali, and W. Villadei, “Orbit determination of resident space objects with the multibeam radar sensor BIRALES,” in *Proc. of the 2018 Space Flight Mechanics Meeting*, 2018.

BIOGRAPHY

Matteo Losacco holds a BSc degree in Aerospace Engineering and a MSc degree in Space Engineering from Politecnico di Milano, and he is currently a Ph.D. student in Aerospace Engineering at the same university. His research is focused on the development of innovative orbit determination algorithms for radar sensors in multibeam configuration. His scientific interests include impact probability computation of Near-Earth Objects using advanced Monte Carlo methods and space trajectories optimization.

Pierluigi Di Lizia is Assistant professor of Aerospace Mechanics at Politecnico di Milano. His current research activity focuses on space surveillance and tracking, nonlinear filtering techniques for pose estimation, and autonomous GNC strategies. Since 2012, he has been collaborating with the team of the Northern Cross radio telescope on the development of orbit determination algorithms for radar sensors in multibeam configuration.

Mauro Massari is Assistant Professor at Politecnico di Milano. His research activities include space trajectory optimisation with direct transcription techniques based on multiple shooting and finite element in time, modern and classical control techniques based both on state space and neural network, and autonomous navigation and obstacles avoidance methods for rovers based on artificial stereo vision system for environment reconstruction and object identification

Germano Bianchi holds a MSc degree in Telecommunication Engineering from the University of Bologna. Since 2002 he has been working as a researcher at IRA-INAF. He has been involved in the technological development project of the new generation radio telescope SKA (Square Kilometre Array), working on digital back end design (signal digitalization, synchronization and processing) and on the correlation of antennas array. Since 2013 he has been in charge of the Northern Cross radio-telescope. He is the chair of the Italian Technical Operating Committee of the European SST Consortium

Giuseppe Pupillo received the MSc degree and the Ph.D. in astronomy from the University of Bologna, Italy, in 1999 and 2003, respectively. In 2007 he joined IRA-INAF, where he is currently working as technologist. He is mainly involved in the framework of the Square Kilometre Array. His current research interests include astronomical low-frequency aperture arrays and bistatic radar systems for space surveillance in the SST program.

Andrea Mattana holds a MSc degree in Automation Engineering from the University of “Roma Tre”. He has been working at INAF since 2000 as a technician. He worked at the “Interplanetary Space Institute of Physics” in Rome as experiment manager of the Italian “Planetary Fourier Spectrometer (PFS)” on board of the ESA Mars Express orbiter. He has been involved in several space missions such ESA/Venus Express and the EXOMARS Rover. He is currently working for IRA-INAF at the Medicina Radio astronomical Observatory as digital back end designer.

Giovanni Naldi received the BSc and MSc degrees in Telecommunications Engineering from the University of Bologna, Italy, in 2003 and 2006, respectively. In 2010 he joined IRAINAF, working on the design of analog receivers for low frequency aperture arrays. Since 2013, he has been a Technology Researcher, involved principally in the framework of the Square Kilometre Array project. His current research interests include testing procedures of digital circuits, numerical simulations of antenna arrays systems and design of firmware blocks for digital signal processing.

Claudio Bortolotti received the Electrotechnical Industrial expert diploma in 1981. Since 1984 he has been an electronic designer and RFI monitoring expert at IRA-INAF. He works for VLBI and the Northern Cross radio telescopes, and he is involved in the Space Debris project.

Mauro Roma joined IRA-INAF in 1984, and he was assigned to the observation service, as well as the maintenance and development of the new VLBI parabolic dish of 32 m and the upgrade of the Northern Cross antenna. He collaborates in the field of Radio Interference (RFI) in the development of new systems of receipt and in the service of search and elimination of interferential causes. He is involved in the project of Sardinia Radio Telescope (SRT) to transfer skills acquired in time-frequency and RFI.

Marco Schiaffino received the MSc degree in Mechanical Engineering from the University of Bologna, in 2005. Since 2005, he has been a Mechanical Project Engineer for the Institute of Radio Astronomy (IRA-INAF), Bologna, where he has been involved in some international projects, such as SKA and SST.

Federico Perini received the MSc degree in Telecommunications Engineering from the University of Bologna in 2001. From 2002 he has been working for IRA-INAF at the Medicina radio telescopes as RF project engineer. His activities are focused on the design and development of RF/IF receivers and signal transportation systems based on RadioFrequency over Fibre (RFoF) technology for both the Italian radio telescopes and international facilities (currently LOFAR2.0 and SKA1-low).

Luca Lama holds a MSc degree in Applied Physics from University of Bologna. He is currently working for IRA-INAF on a H2020 Space Surveillance and Tracking project as technological researcher.

Alessio Magro is a lecturer at the Institute of Space Sciences and Astronomy, University of Malta. His main research topic is the design and implementation of high performance software back ends for radio instruments, focusing on the low frequency component of the Square Kilometre Array (the Low Frequency Aperture Array). He is involved in several international projects, including the LFAA, PHAROS2 (a new pixel feed being design for SKAmid) and BIRALES.

Denis Cutajar obtained a BSc in Physics and Computer Science from the University of Malta in 2012. This was followed by a Master in Physics obtained in 2014. At present, he is reading for a PhD in Space Sciences at the Institute of Space Sciences and Astronomy of the University of Malta. His research focuses on the application of machine learning techniques for the detection of orbital debris using radar instruments.

Josef Borg graduated in a dual honours degree, reading for biology and chemistry within the Faculty of Science at the University of Malta, with the undergraduate dissertation focusing on astrochemistry. Currently, he is reading for a PhD in radio astronomy, focusing on precision calibration of radio interferometers. Since 2016, he has been working on developing calibration pipelines for both the Square Kilometre Array and the BEST-2 array of the Northern Cross.

Ten. Col. G.A.r.n. Walter Villadei is a graduate of the Italian Air Force Academy and holds a Master Degree in Aerospace Engineering from the University Federico II of Napoli. He is currently the head of the Innovation, Systems and Space Applications department of the Force Space Policy Office of the Italian Air Force.

Magg. G.A.r.n. Marco Reali is a graduate of the Italian Air Force Academy. He is currently working for the Force Space Policy Office of the Italian Air Force.